

Backbone curve variations on steel building seismic response

Bruce Maison,¹ Matthew Speicher,² Dimitrios Lignos³

Abstract: A four-story steel moment-frame building designed according to ASCE 7 was used in a numerical parameter study to assess the effects of modeling features on peak drift demands. Features studied included strength, stiffness, ductility, and degradation along with several hysteretic models. Attention was given to ASCE 41 type backbone curves. Of particular interest was exploring the effects of degradation, in which an adaptive backbone curve was used to capture both in-cycle and cyclic degradation. Incremental dynamic analyses (IDA) were performed using a suite of earthquake records to assess the response over a range of shaking intensities. It was found that in-cycle degradation had more influence on the response compared to cyclic degradation for the set of ground motion records that were employed. Moreover, use of the monotonic backbone alone, with its in-cycle degradation, was sufficient. Additionally, it was found that increasing strength, stiffness, and/or ductility resulted in decreased peak drift demands, whereas modifying the hysteretic type (elasto-plastic, stiffness-degrading, and pinching) had little effect on peak drifts. These findings indicate that using backbone curves based on envelopes of first-cycle test data, as done in ASCE 41, can result in overly-conservative seismic response predictions.

Introduction

Performance-based engineering, in which a structure is proportioned to meet certain predictable performance objectives, requires knowledge of component (e.g., steel beam-to-column connection) inelastic behavior during earthquakes. The ASCE 41 performance-based standard (ASCE 2017), *Seismic Evaluation and Retrofit of Existing Buildings* uses

¹ Consulting Engineer, El Cerrito, CA 94530

² Research Structural Engineer, National Institute of Standards and Technology, Gaithersburg, MD 20899

³ Professor, École Polytechnique Fédérale de Lausanne (EPFL), Station 18, Lausanne 1015, Switzerland

a force-deformation *backbone* curve to describe component ultimate force over a range of deformations as depicted in Figure 1. ASCE 41 modeling and acceptance requirements for deformation-controlled components are based on backbones usually taken as envelopes from multiple cyclic tests thereby implicitly including cyclic deterioration.

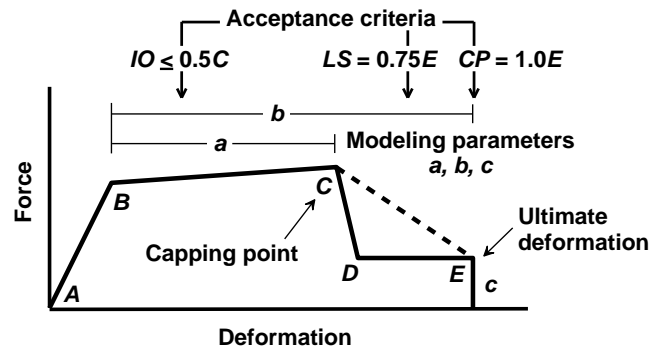


Figure 1. ASCE-41 component backbone curve (force-deformation relationship). IO, LS and CP indicate acceptable deformation limits for immediate occupancy, life safety, and collapse prevention structural performance objectives, respectively. Acceptance criteria are dependent on capping point (C) and ultimate deformation (E).

For building evaluation using the nonlinear dynamic procedure (NDP), various structural components are modeled using backbone curves that influence response predictions and in turn determine whether components have acceptable seismic performance. Backbone curves are key factors in ASCE 41.

This article examines the influence of modeling features on the peak drift demands obtained using the NDP. A parameter study is conducted using a single-degree-of-freedom (SDOF) approximation of a four-story steel moment-frame case study building. Conclusions are drawn regarding the impact of modeling variations on computed peak building drifts. The information presented herein is intended to inform performance-based engineering practice.

Case Study Building

Numerous archetype steel buildings were studied extensively as part of the National Institute of Standards and Technology (NIST) project *Assessment of First Generation Performance-Based Seismic Design Methods for New Steel Buildings*. NIST evaluated the buildings using ASCE 41 and P695 criteria. ASCE 41 evaluations used the ASCE 41 prescribed modeling (backbone curves) and acceptance rules. The P695 evaluations used modeling techniques intended to best capture actual building behaviors, and defined

acceptance by a particular probability of collapse (FEMA 2009a, NIST 2017). It was found that ASCE 7-10 (ASCE 2010) designed buildings were rejected by ASCE 41, but passed evaluations using the P695 guidelines. It was then concluded ASCE 41 can be overly conservative.

The building considered here was the four-story moment-frame building having reduced beam section (RBS) connections (Figure 2). Full details can be found in NIST reports (Harris and Speicher 2015, Speicher et al. 2020).

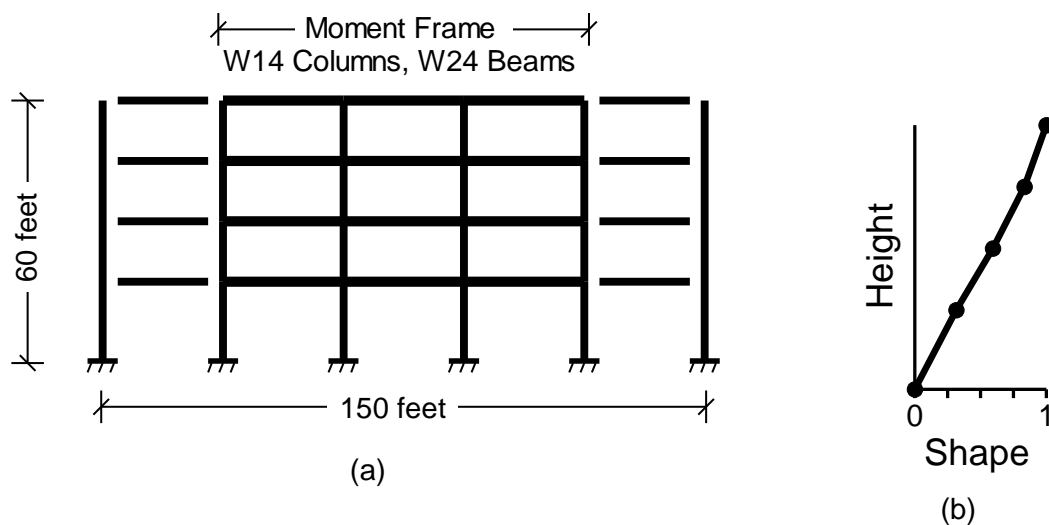


Figure 2. Case study building. (a) Elevation view depicting structural system located on building exterior column line. (b) Shape function (Ψ) taken as fundamental mode shape.

Nonlinear Model

The P695 evaluation by NIST analyzed a detailed member-by-member building model using the *OpenSees* software (McKenna and Fenves 2016). A simplified model based on the detailed model was used here. It allowed for efficient execution of numerous NDP computer runs. The simplified model used the first mode (Figure 2b) as a shape function to define the building lateral displacements. This was deemed appropriate since the *OpenSees* analyses found negligible column hinge yielding except at the fixed end first story columns. Because the columns stayed mostly elastic, the lateral sway pattern was similar to a first mode shape. Most inelastic actions occurred in the RBS connections with much less yielding in column panel zones.

The simplified model was thus a generalized nonlinear SDOF approximation of the detailed *OpenSees* model. The generalized coordinate was set at the building roof, and the building inelastic actions were conveniently accounted for by a single generalized backbone curve describing the building global nonlinear behavior. Since RBS connection inelastic actions predominated, the global backbone curve mostly reflects the aggregated RBS connection behaviors. Response measures were median peak transient *forward* and *reverse* building deformations taken as roof drifts (roof displacement divided by the building height, expressed as a percentage). The forward direction was defined as that having the largest roof drift. Model properties are explained in Exhibit 1.

Exhibit 1. Equation of motion in generalized coordinate parameters.

The parameters were based on the formulation by Clough and Penzien (1975), and the solution for the nonlinear time history of response used the method by Newmark (1962) implemented into a custom computer program. The equation of motion is as follows.

$$m^*a + c^*v + (k^* + k_G^*)d = p^*a_g$$

a = generalized acceleration coordinate (relative to base).

v = generalized velocity coordinate.

d = generalized displacement coordinate.

m^* = generalized mass = 3.42 kip-sec²/in

c^* = damping coefficient set to 3% viscous damping at the fundamental frequency with the force capped at 6% of the backbone ultimate force to negate unrealistically large damping forces after yielding (Hall 2006).

k^* = generalized nonlinear stiffness. This changes during an analysis run as explained in the Generalized Backbone Curve section. Base case initial stiffness set to have a building period of 1.8 sec to match detailed *OpenSees* model.

k_G^* = generalized geometric stiffness (P-delta effect) = -2.57 kip/in.

p^* = generalized earthquake loading mass = 4.47 kip-sec²/in.

a_g = ground acceleration.

$$m^* = \sum_{i=1}^{n=4} m_i \Psi_i^2; \quad k_G^* = \int_0^H N(x) \Psi'(x)^2 dx; \quad p^* = \sum_{i=1}^{n=4} m_i \Psi_i; \quad F^* = \sum_{i=1}^{n=4} F_i \Psi_i$$

m_i = mass at level i in building.

$N(x)$ = vertical gravity force distribution over building height.

F^* = generalized pushover force.

F_i = pushover force at level i .

Ψ_i or $\Psi(x)$ = shape function taken as first mode shape (Figure 2b taken from Figure 67 in Speicher et al. 2020).

n = number of levels in building = 4.

H = distance from base to generalized coordinate at roof.

Strength Degradation Models

The detailed *OpenSees* model used *adaptive* modeling via the modified Ibarra-Medina-Krawinkler (IMK) formulation in which a component starts with a reference monotonic backbone curve that is degraded during the NDP analysis according to the accumulated inelastic deformation history (Ibarra et al. 2005, Lignos and Krawinkler 2012). It captured both in-cycle and cyclic degradation in flexural strength and unloading stiffness. In-cycle degradation (FEMA 2009b) is characterized by loss of strength occurring within a single cycle (e.g., during a monotonic push). Cyclic degradation is defined as loss of strength and stiffness from reversed cyclic displacements.

It should be noted that the *OpenSees* model was formulated to best capture actual building response and was *not* an ASCE 41 model. Adaptive modeling is not often used in engineering practice. ASCE 41 prescribed backbone curves are typically based on first-cycle envelopes of standard fully reversed cyclic test data thereby including cyclic degradation (Krawinkler 1996, NIST 2017). They are intended for use in customary state-of-practice analysis software that lacks adaptive modeling capabilities. As shown later, building earthquake response resulted in negligible cyclic degradation thereby making the ASCE 41 backbones very conservative (too pessimistic).

The generalized nonlinear SDOF model here also used an adaptive approach via a simple yet effective empiric model (Maison et al. 2020). The adaptive model separated in-cycle and cyclic effects as explained below. Validation was demonstrated by comparison to physical component tests in the Appendix and Supplemental Materials file.

In-Cycle. Strength degradation was controlled by a backbone curve acting as a capacity boundary (Figure 3a). The hysteretic behavior was elasto-plastic and as the deformation increased, the ultimate force progressively decreased according to the backbone curve. The backbone was taken as the curve from a monotonic loading, or a skeleton curve constructed from the decomposition of cyclic lab test data. A skeleton curve consists of an envelope of horizontally shifted hysteretic loops resembling a monotonic curve as explained by Maison et al. (2020).

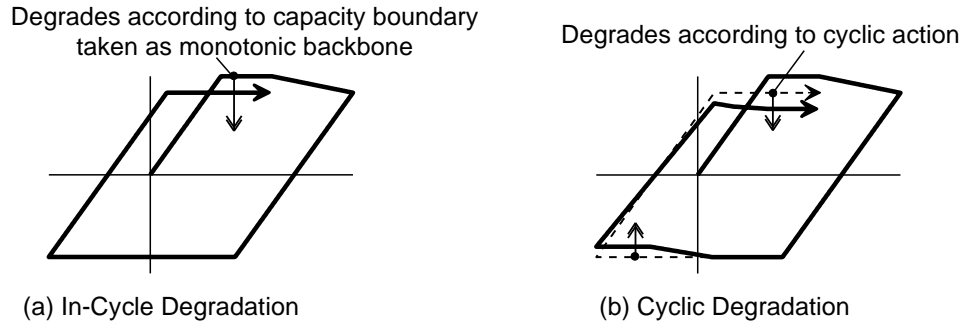


Figure 3. Illustration of adaptive model in-cycle and cyclic strength degradation features.

Cyclic. Strength degradation was modeled as a force reduction dependent on the amount of cyclic action (Figure 3b). Cyclic action (*CA*) was defined as the *minimum* of the cumulative plastic deformations in the positive and negative directions as the analysis proceeded. In essence, *CA* was a measure of the amount of plastic deformation reversal. The force from the in-cycle part above was scaled by a factor (*SF*) taken from a cyclic action curve (Figure 4). Scaling occurred continuously as the plastic deformations accumulated during the NDP analysis run. It was found that the cyclic action curve can be conveniently based on the part of the backbone curve beyond point B (Figure 1) as illustrated in the Appendix.

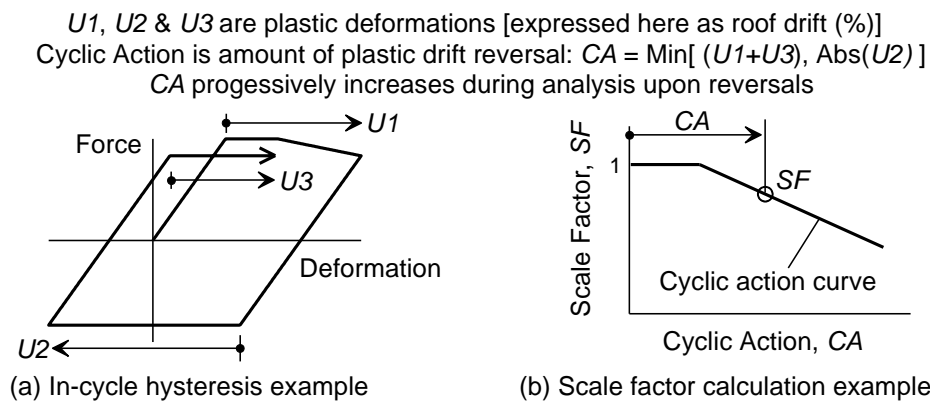


Figure 4. Example depicting how adaptive model cyclic degradation algorithm works for determination of force scale factor (*SF*). *SF* is applied to in-cycle force part to get component force.

Generalized Backbone Curve. The generalized stiffness (k^*) was modified during an analysis according to the adaptive model described above. In-cycle degradation was accounted for by the backbone derived via the monotonic pushover from the detailed *OpenSees* model that used a lateral force pattern according to the first mode shape

(Figure 5a). The pushover curve was transformed to the generalized coordinate as explained in Exhibit 1 (equation for F^*). The generalized backbone mostly reflected the aggregated RBS connection monotonic behaviors. Cyclic degradation was accounted for by the cyclic action curve shown in Figure 5b.

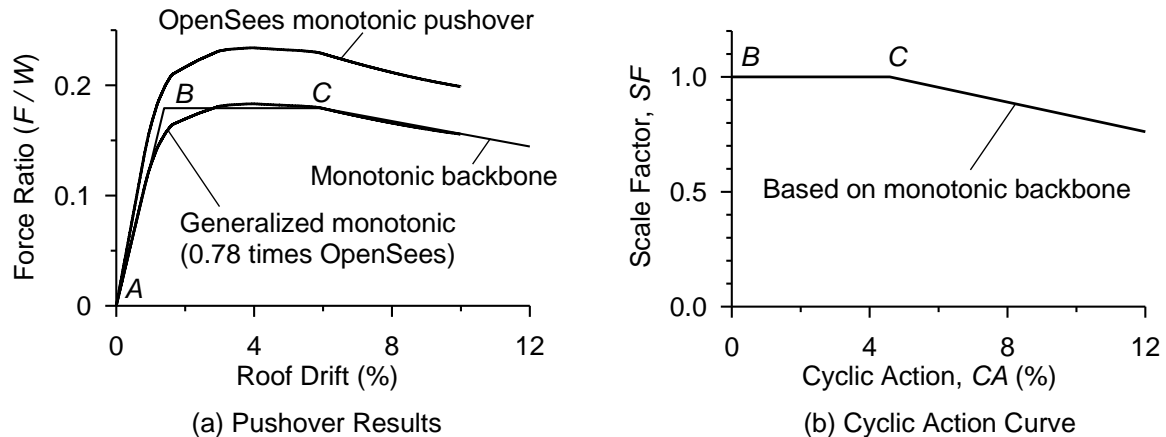


Figure 5. Base case building generalized stiffness (k^*). (a) Monotonic backbone curve is the piecewise linear representation of generalized monotonic pushover. *OpenSees* curve is the pushover *without* P-delta effects because P-delta is applied separately in the generalized building model. The 0.78 factor transforms the *OpenSees* pushover forces to an equivalent force at the generalized coordinate per equation for F^* in Exhibit 1. W = total building weight. (b) Cyclic action curve. The cyclic action curve shape is taken as that part of the backbone curve beyond point *B*.

Ground Motions

A suite of ground acceleration records was used representing a high-seismicity site that might experience strong ground motions from mid- to large-magnitude earthquakes at close distances. The suite, which is comprised of 80 horizontal records, represents earthquakes having a 2% probability of exceedance in 50 years (2500-yr events) at a soil site (site class C/D) in the city of Oakland, California (Baker et al. 2011). The site was close enough to the governing fault thus potentially experiencing directivity effects, and 19 records (1 in 4 records) have velocity pulses with pulse periods between one and seven seconds. The median spectrum greatly exceeded the design basis earthquake (0.67 times the maximum considered earthquake) used for the building (Figure 6).

Since the acceleration records varied, the computed peak building responses had scatter. Thus, the counted medians of the peak values were used as best estimates (the peak value in the middle).

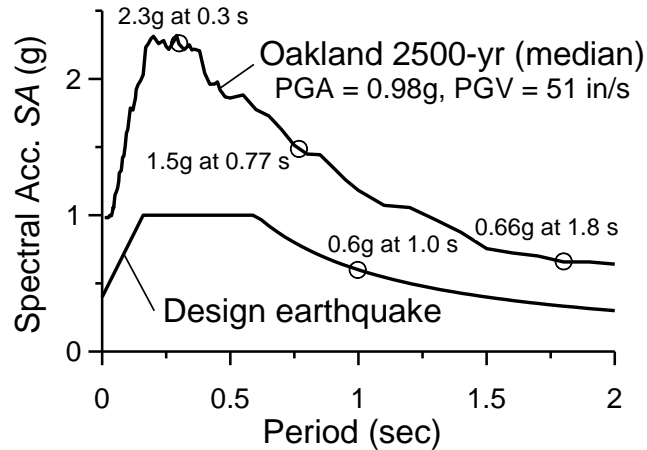


Figure 6. Response spectra (5% damping). PGA and PGV are median peak ground acceleration and velocity, respectively. Building was designed by the equivalent lateral force method using a period of 1.0 s.

In-Cycle vs. Cyclic Degradation

The base case simplified SDOF model used adaptive modeling and was intended to mimic actual building behaviors. It did *not* use ASCE 41 prescribed backbone curves. The simplified model was subjected to the suite of 80 records scaled to the 2500-yr intensity. The building responded with pronounced one-direction bias (i.e., ratcheting behavior). The median peak forward roof drift of 4.6% was about three-times that of the reverse direction (Figure 7a). The numbers of inelastic cycles during the response history (cumulative plastic deformation reversals) were small, and thus, there was no cyclic degradation at the median run (Figure 7b). Hence, cyclic degradation was minimal and the response essentially followed the in-cycle (monotonic) backbone. Sample analyses of the detailed *OpenSees* building model had the same conclusion when re-run with the cyclic degradation feature turned off. This corroborates with findings of shake table and quasi-static collapse tests of a scale model of a 4-story steel moment-frame specimen having similar strength characteristics (Lignos et al. 2011, Del Carpio et al. 2016). Lack

of significant fully reversed cyclic action in building seismic response was also noted previously (e.g., Krawinkler 2009, Maison and Speicher 2016).

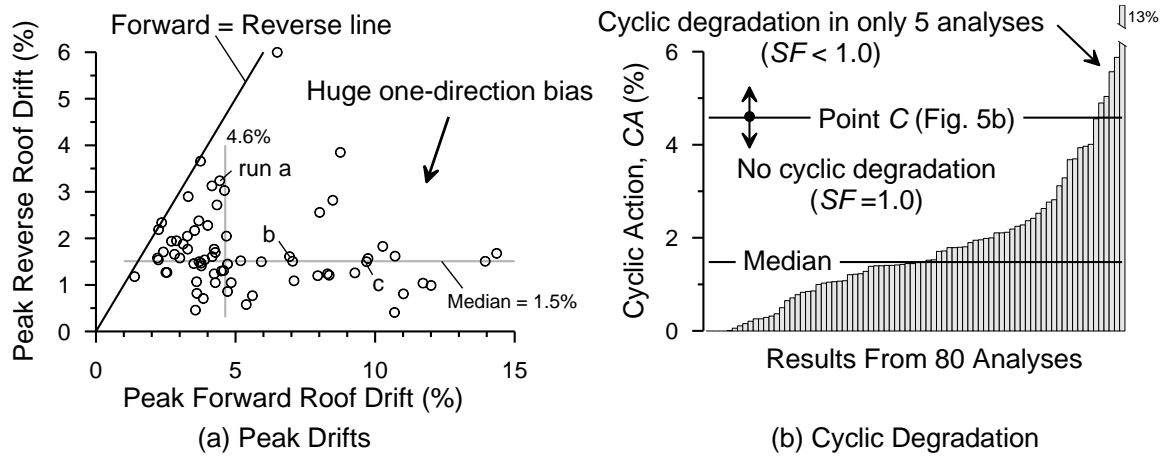


Figure 7. Results from base case model subjected to 80 records from Oakland 2500-yr earthquake suite. (a) Peak forward and reverse drifts exhibiting a one-direction bias via ratcheting response as explained in text. Eleven runs had building collapse and data points not shown (large forward drifts). (b) Cyclic degradation. See Figure 5b for cyclic action curve.

Figure 8 shows response history results from three analysis runs illustrating representative response patterns. Peak reverse drift occurred early in the response after which the building experienced an inelastic reversal to the forward direction. The behavior exhibited a ratcheting response in that the building progressively drifted in one direction via relatively few incremental inelastic excursions interspersed with mostly elastic cycles. The destabilizing effects of gravity (k_G^*) bolstered ratcheting after yielding in the forward direction by reducing the effective yield force in the forward direction while increasing it in the reverse direction (creating asymmetric yield forces). Longer duration earthquakes would be more hazardous provided the shaking had sufficient intensity to cause additional inelastic excursions. Response was like a one-sided cyclic pattern or monotonic push rather than standard fully reversed symmetric cyclic loading patterns (protocols) commonly used in component lab tests that served as the basis of many ASCE 41 prescribed backbone curves.

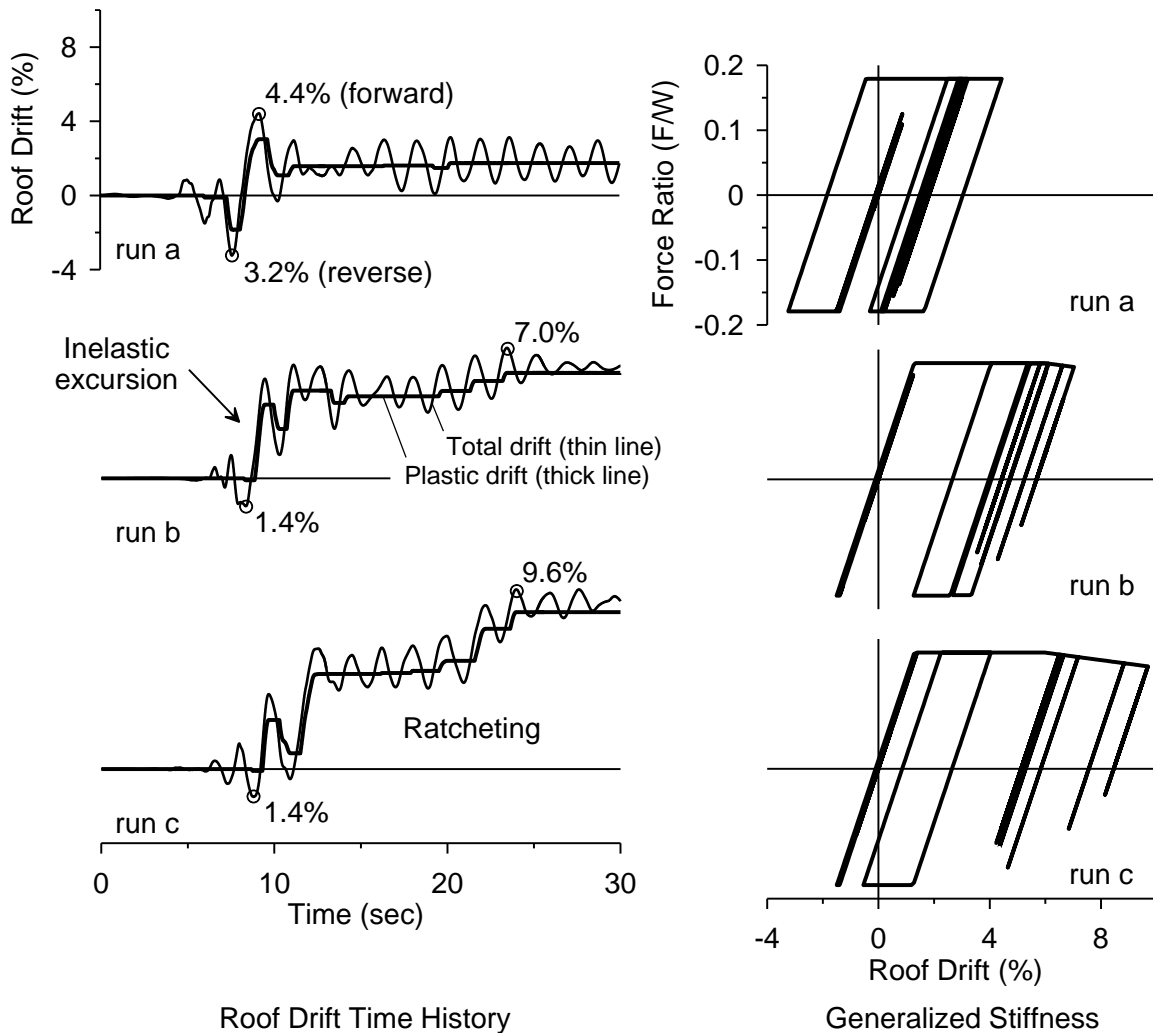


Figure 8. Sample time history results from three earthquake analyses of the generalized building model. Notice how the plastic drift response resembles a monotonic pushover. Runs selected are indicated in Figure 7a.

Variations in Model Properties

Additional NDP analyses of the simplified SDOF building model were performed to assess the effects of model property variations on median computed peak roof drift demands. Cyclic action curves were set corresponding to the particular backbone curves even though cyclic degradation was found to be insignificant. To provide insights about response over a range of shaking intensities, incremental dynamic analysis (IDA) was performed via scaling the earthquake suite. Median results were reported here, since it is customary to use best estimates of peak response in performance-based engineering (e.g.,

ASCE 41 uses average peak values in NDP). Variability about the median at particular shaking intensities was not considered, although it is expected to be similar across the different cases studied.

Ductility. The results from three models were compared: (1) *base case* with the backbone explained above, (2) *RBS case* having the backbone based on ASCE 41 prescribed parameters for RBS connections (*a*, *b*, *c* in Figure 1), and (3) *WUF case* having the backbone based on ASCE 41 prescribed parameters for unreinforced flange (WUF) connections. Figure 9a show the backbones. The RBS and WUF backbones can be considered to represent upper and lower bounds, respectively, on ASCE 41 prescribed connection ductility. They have much less ductility than the base case because cyclic degradation was implicitly included.

Figure 9b shows the IDA results. All three models had the same median peak drifts until capping points were exceeded. The base case model governed by the monotonic backbone had 1.3-times and 1.8-times greater ultimate shaking intensity and drift capacity than the RBS case, respectively (comparing base case to RBS in Figure 9b).

The base case withstood shaking intensities larger than those for the RBS and WUF cases because of its greater ductility. The base case and RBS case had about the same capping points (point C); hence, the better base case response at high intensity shaking was due to the more gradual post-capping slope of the backbone. Thus, component ductility depended on both the capping point deformation and the slope of the backbone beyond the capping point. This underscores the importance of backbone ductility.

Moreover, suppose the building was analyzed using adaptive modeling, but evaluated under current ASCE 41 acceptance criteria. The CP deformation limit would be about 7.7% roof drift given that RBS connections govern (Figure 9a), whereas the base case adaptive model was able to sustain at least 1.4-times greater drift without collapse (11% roof drift, Figure 9b). The building could be rejected because the ASCE 41 CP acceptance criterion was based on standard tests. Therefore, ASCE 41 acceptance criteria should be based on backbones derived from physical tests representative of actual earthquake demands.

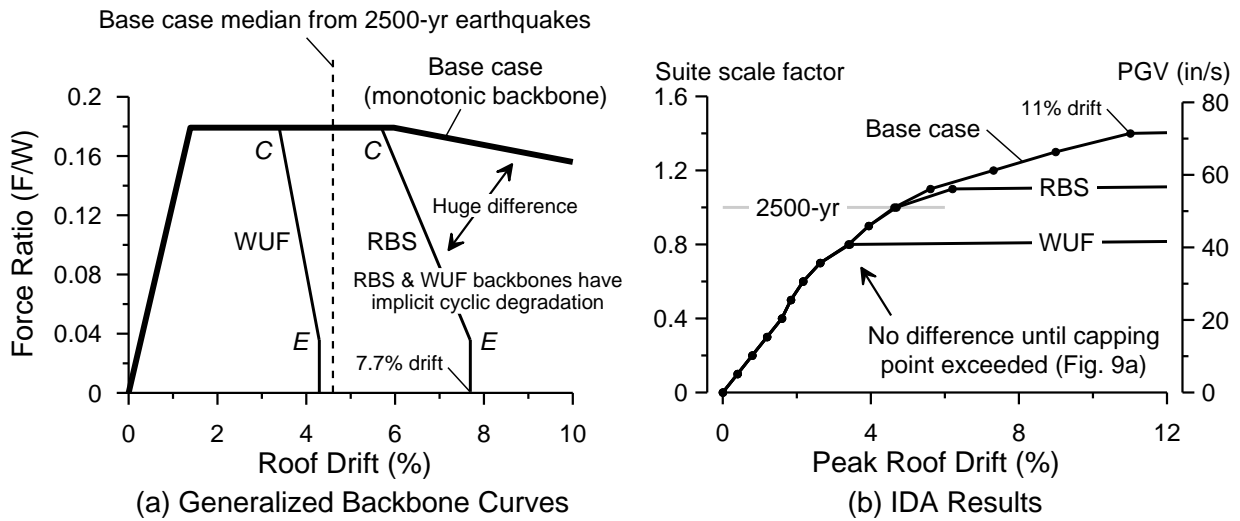


Figure 9. Effect of ductility on median peak drifts. (a) Building generalized backbone curves. RBS and WUF capping point *C* and ultimate point *E* based on ASCE 41 modeling parameters (Table 9-7.2) for RBS ($a = 0.043$ rad, $b = 0.063$ rad, $c = 0.2$) and WUF ($a = 0.02$ rad, $b = 0.029$ rad, $c = 0.2$) connections, respectively. Roof drift ratio was taken as equivalent to connection hinge rotation. (b) IDA results. Each data point (dot) is the median of 80 computer runs at the particular Oakland suite scale factor. For example, when the suite was scaled by 0.8 (80% of the 2500-yr intensity), all models had the same median peak roof drift of 3.4%. Graph represents results from more than 1400 runs.

Hysteretic Type. Results from three models using different hysteretic behaviors (all using base case backbone) were compared: (1) *base case* using elasto-plastic hysteretic type, (2) *stiffness-degrading case*, and (3) *pinching case*. Figure 10a depicts the hysteretic types. Elasto-plastic is often used to describe steel component behavior. Stiffness-degrading (sometimes called peak-oriented) is often used for concrete components such as beams and columns. Pinching is often used for squat concrete shear walls, and for wood components such as plywood shear walls.

Hysteretic type had only modest impact on median peak drifts (Figure 10b). This was because the inelastic response consisted mostly of a series of one-sided excursions that follow the initial elasto-plastic backbone shape (Figure 8) rather than large fully reversed hysteretic loops depicted in Figure 10a. Ibarra and Krawinkler (2005) numerical studies of generic frames suggests the same conclusion. For the severe pinching model used here (having zero strength upon load reversal), the median peak drifts were about 30% greater

than the base case at the 2500-yr intensity. Stiffness-degrading had virtually the same median drifts as the base case at the 2500-yr intensity. Ironically, stiffness-degrading performed better (smaller drifts) than the base case under very high intensity shaking. This is likely due to stiffness-degrading mitigation of ratcheting by having reduced stiffness upon load reversals thereby allowing a building self-centering effect, which is consistent with prior findings (Ibarra and Krawinkler 2005).

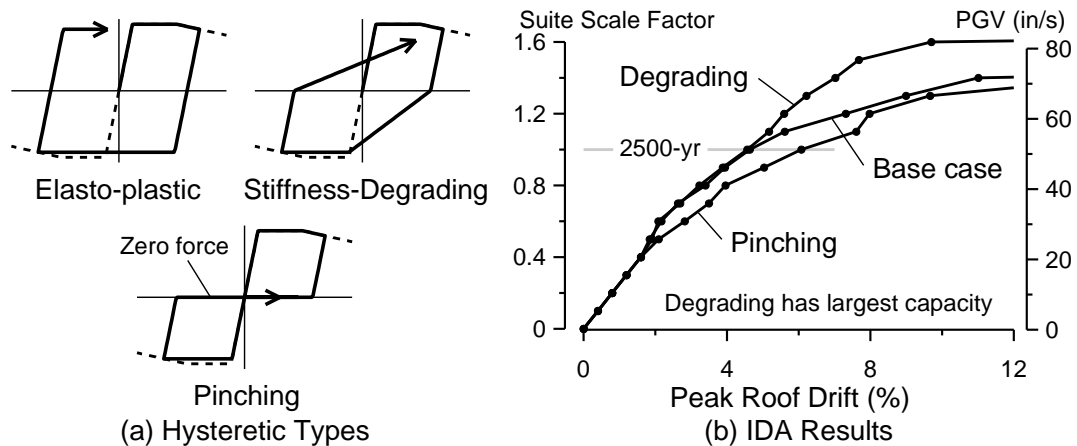


Figure 10. Effect of hysteretic type on median peak drifts. (a) Three different types of hysteretic behaviors. Base case used elasto-plastic. (b) IDA results. Each data point (dot) is the median of 80 computer runs at the particular Oakland suite scale factor.

Lateral Strength. The results from two models were compared: (1) *base case* with the backbone explained above, (2) *reduced-strength case* having ultimate lateral strength (ultimate base shear) set at two-thirds of the base case. Figure 11 shows the backbones and IDA results. The median peak drifts progressively diverged with increasing deformations beyond the yield drift (Figure 11b). The reduced-strength building experienced greater ductility demands at a given intensity than the base case. It had a median shaking intensity causing side-sway collapse about 30% less than that for the base case. Hence, greater strength translated into better performance.

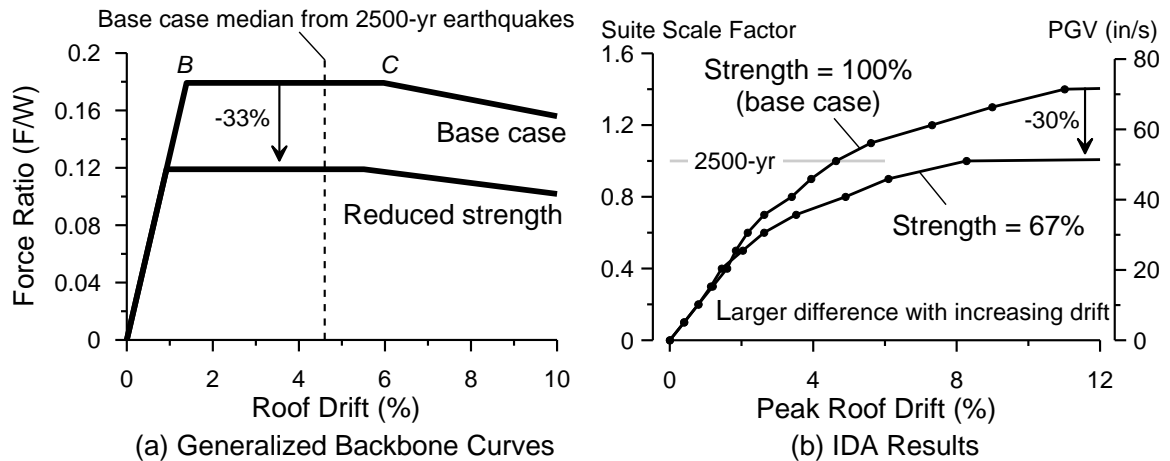


Figure 11. Effect of ultimate lateral strength on median peak drifts. (a) Backbone curves. (b) IDA results. Each data point (dot) is the median of 80 computer runs at the particular Oakland suite scale factor.

Building Period. The base case model had fundamental natural period of 1.8 sec that was considerably greater than that from the ASCE 7 formula ($C_u T_a = 1.0$ sec), and regression equations from actual building measurements (0.74 sec (lower) to 1.2 sec (upper) per Goel and Chopra (1997)). Possible reasons for discrepancy include customary practice of ignoring stiffness contributions from slab-girder composite action, gravity frames, and nonstructural components. Such features can contribute significantly to the lateral stiffness of a steel frame building (for example, see Elkady and Lignos 2014, 2015, Flores et al. 2016, Maison and Neuss 1985).

The results from three models having different periods were compared: (1) *base case* with period $T = 1.8$ sec case (set to match the detailed *OpenSees* model), (2) $T = 0.77$ sec case having five-times the base case stiffness, and (3) $T = 0.3$ sec case having thirty-six times the base case stiffness. Figure 6 illustrates the wide variation in spectral accelerations associated with the different periods.

Figure 12 shows the backbone curves and IDA results. The $T = 0.77$ sec case resulted in smaller median peak drifts at all shaking intensities versus the base case (Figure 12b). It had 36% less drift at the 2500-yr intensity. The $T = 0.3$ sec case resulted with the smallest median peak drifts at all shaking intensities. Greater stiffness more than offset the increase in spectral values (Figure 6). Hence, ignoring stiffness contributions in NDP evaluation produced conservative drift estimates (i.e., on the high side).

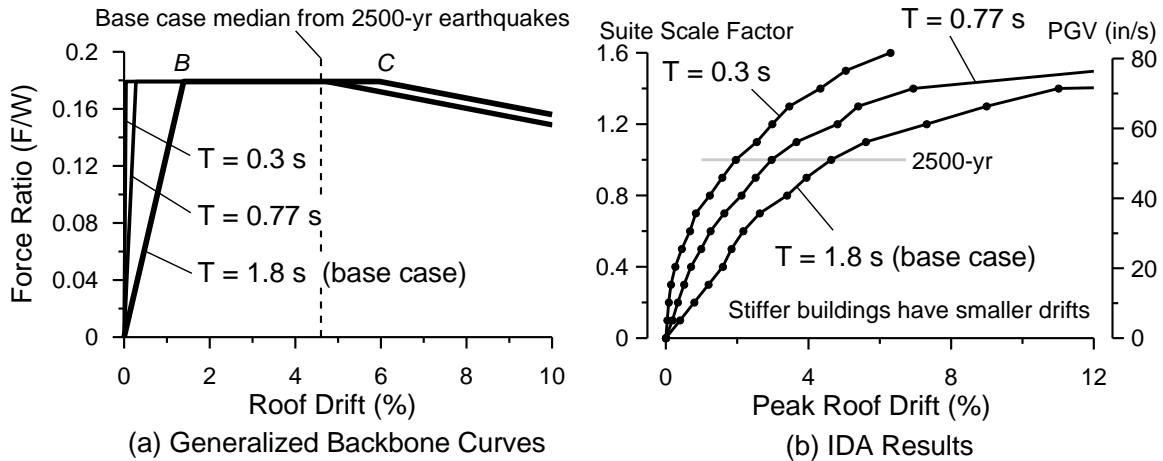


Figure 12. Effect of building period (stiffness) on median peak drifts. (a) Backbone curves. (b) IDA results. Each data point (dot) is the median of 80 computer runs at the particular Oakland suite scale factor.

Discussion

Many of the findings here were reported previously by other researchers (see reference sources in Maison and Speicher 2016, Speicher and Maison 2020). The prior work was motivation for the current study to validate and underscore key findings for the benefit of practicing engineers. Two important aspects are highlighted below.

Adaptive Modeling. It was found here that adaptive component modeling was not needed for the cases considered. Cyclic actions were minimal thus leading to little cyclic degradation (Figure 7b). Accordingly, building behavior was governed by in-cycle degradation represented as the monotonic backbone. Previously, authors of the IMK adaptive model did extensive parameter studies and found that backbone ductility capacity (capping point C deformation) and post-capping stiffness were most influential in building side-sway collapse when compared to cyclic degradation that had smaller effect (Ibarra and Krawinkler 2005). Likewise, the Applied Technology Council ATC-62 project, *Effects of Strength and Stiffness Degradation on Seismic Response*, found in most cases, the effects of in-cycle strength degradation dominate the nonlinear dynamic

behavior suggesting that effects of cyclic degradation can often be neglected (FEMA 2009b).

ASCE 41 Backbones. Many (perhaps most) of the ASCE 41 component criteria were based on physical tests using standard fully reversed symmetric cyclic loading patterns (e.g., ATC 1992 protocol). It was noted here that such protocols produce cyclic degradation that is more demanding than representative seismic response (Figure 13), and building models using ASCE 41 backbones having implicit cyclic degradation can be overly conservative (too pessimistic). Previously, Lignos and Krawinkler (2012) found the use of standard protocols provides insufficient information for component degradation modeling near collapse, and that alternative loading protocols were needed. This led to Suzuki and Lignos (2020, 2021) proposing a collapse-consistent protocol representing realistic earthquake demands. Use of protocols representative of actual earthquake demands likely will result in backbone curves having more ductility than many of those prescribed in ASCE 41.

Moreover, the Applied Technology Council ATC-116 project, *Short-Period Building Collapse Performance and Recommendations for Improving Seismic Design* necessitated use of backbone curves having much more ductility than those of ASCE 41 in order to explain the observed better-than-expected performance of short-period buildings (FEMA 2020). Conservative modeling was one of the reasons for the “short-period paradox.” It also recommended that a study be undertaken to review and update existing cyclic-load testing protocols to better reflect real earthquake loading conditions.

It follows that modeling and acceptance criteria can be overly conservative when based only on standard tests (i.e., understate component ductility during earthquakes). This undoubtedly contributed to ASCE 7 designed buildings being rejected by ASCE 41 (Harris and Speicher 2015).

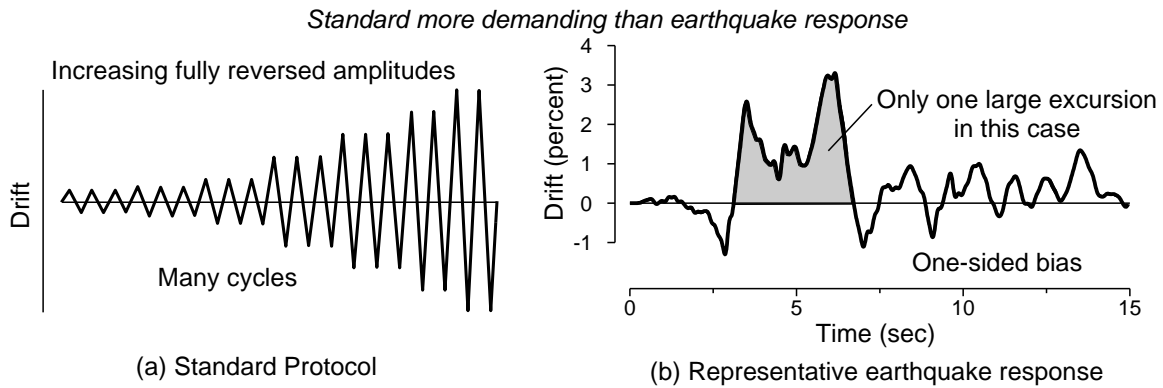


Figure 13. Comparison of standard loading protocol to representative building seismic response for an 8-story EBF steel frame building (Maison and Speicher 2016).

Conclusion

A four-story steel moment-frame building designed according to ASCE 7 was used in a parameter study to assess the effects of modeling variations in NDP evaluation for best estimate (median) peak building drift demands. The building model incorporated an adaptive component formulation to account for in-cycle and cyclic strength degradation. It is reasonable to expect the following apply to similar buildings in analogous seismic settings, thereby informing performance-based engineering practice.

(1) The case study building's inelastic strength degradation was mostly from component in-cycle effects (Figure 3a). Cyclic degradation was minimal (Figure 7b), and thus in-cycle degradation governed the response. Hence, adaptive modeling was not needed. It was adequate to use the monotonic backbone curve alone rather than a backbone from envelope of standard tests that includes cyclic degradation.

(2) Better performance (smaller median peak drifts) was obtained when the building backbone curve had larger ductility (larger capping point deformation and more gradual post-capping slope). The case study building capping point was at about 6% roof drift (Figure 9).

(3) Hysteretic behavior type had relatively small effect on median peak drifts (Figure 10, elasto-plastic, stiffness-degrading, pinching). Stiffness-degrading hysteretic behavior

had the best performance (often used to model concrete components), which was likely due to the mitigation of ratcheting by having reduced stiffness upon load reversals.

(4) Better performance was obtained when the building had larger ultimate lateral strength (ultimate base shear) and/or shorter period (Figures 11 and 12). This implies it was conservative to ignore features contributing strength and stiffness to the building (i.e., resulting drift predictions on the high side).

(5) The building experienced ratcheting where it progressively drifted in one direction via relatively few incremental inelastic impulsive excursions (Figure 8). Such behavior was better described as a one-sided cyclic pattern or monotonic push rather than standard fully reversed symmetric cyclic loading patterns (protocols) commonly used in component physical tests.

(6) The distinctive sharp decline in ASCE 41 backbones (beyond the capping point) were largely artifacts of the standard protocols used in component tests (Figure 1). Standard protocols produce component cyclic degradation *not* characteristic of actual earthquake demands. Resulting modeling and acceptance criteria likely underestimate component seismic performance. This undoubtedly contributed to the case study building being rejected by ASCE 41.

(7) Future component physical tests in support of performance-based engineering should include protocols representative of earthquake response (e.g., Suzuki and Lignos 2020) to supplement standard tests. The results at large inelastic (post capping) deformations can be expected to be closer to those from monotonic tests as opposed to standard tests. Latest editions of ASCE 41 now encourage use of protocols representative of earthquake demands to supplement standard tests.

Acknowledgment

The authors are members of the Lab Testing Working Group within the ASCE/SEI Standards Committee responsible for ASCE 41. The authors appreciate valuable input provided by members of the Standards Committee. The authors also appreciate the thorough critiques provided by Dr Siamak Sattar (NIST) and the two anonymous peer reviewers.

Certain commercial software has been used in the preparation of information contributing to this paper. Identification in this paper is not intended to imply recommendation or endorsement by NIST, nor is it intended to imply that such software is necessarily the best available for the purpose.

References

American Society of Civil Engineers (ASCE) 2010. *Minimum Design Loads for Buildings and Other Structures*. ASCE Standard ASCE/SEI 7-10, Reston, VA.

American Society of Civil Engineers (ASCE) 2017. *Seismic Rehabilitation of Existing Buildings*. ASCE Standard ASCE/SEI 41, Reston, VA.

Applied Technology Council (ATC). 1992. *Guidelines for Seismic Testing of Components of Steel Structures*, ATC-24, Redwood City, CA.

Baker J, Lin T, Shahi S and Jayaram N. 2011. *New Ground Motion Selection Procedures and Selected Motions for the PEER Transportation Research Program*. PEER Report 2011/03, Pacific Earthquake Engineering Research Center, Berkeley, CA, March.

Cough, R. and Penzien, J., 1975. *Dynamics of Structures*, section 2-6, McGraw-Hill, Inc.

Del Carpio MR, Mosqueda, G, and Lignos, DG, 2016. Seismic performance of a steel moment frame subassembly tested from the onset of damage through collapse, *Journal of Earthquake Engineering and Structural Dynamics*, DOI: 10.1002/eqe.2743

Elkady, A, and Lignos, DG 2014. Modeling of the composite action in fully restrained beam-to-column connections: implications in the seismic design and collapse capacity of steel special moment frames, *Earthquake Engineering and Structural Dynamics*, 43(13): 1935

Elkady, A, and Lignos, DG 2015. Effect of gravity framing on the overstrength and collapse capacity of steel frame buildings with perimeter special moment frames, *Earthquake Engineering and Structural Dynamics*, 44(8): 1289-1307.

Federal Emergency Management Agency (FEMA). 2009a. *Quantification of Building Seismic Performance Factors*. FEMA Report P695, Washington, D.C.

Federal Emergency Management Agency (FEMA) 2009b. *The Effects of Strength and Stiffness Degradation on Seismic Response*, Technical Report FEMA P-440A, Washington D.C.

Federal Emergency Management Agency (FEMA) 2020. *Short-Period Building Collapse Performance and Recommendations for Improving Seismic Design*, Technical Reports FEMA P-2139-1, -2, -3, Washington D.C.

Flores, F, Charney F, and Lopez-Garcia D 2016. The influence of gravity column continuity on the seismic performance of special steel moment frame structures, *Journal of Constructional Steel Research*, 118, 217–230

Goel RK, and Chopra AK. 1997. Period formulas for moment-resisting frame buildings, *Journal of Structural Engineering*, American Society of Civil Engineering, vol 123, November, pp 1454-1461.

Hall JF. 2006. Problems encountered from the use (or misuse) of Rayleigh damping. *Journal of Earthquake Engineering and Structural Dynamics* 35: 525–545.

Harris JL , and Speicher MS 2015. *Assessment of First Generation Performance-Based Seismic Design Methods for New Steel Buildings Volume 1: Special Moment Frames*. National Institute of Standards and Technology, Gaithersburg, MD, NIST Technical Note 1863-1. <https://doi.org/10.6028/NIST.TN.1863-1>

Ibarra, LF, and Krawinkler, H. 2005. *Global Collapse of Frame Structures Under Seismic Excitations*, Stanford University Blume Earthquake Engineering Center Report No. 152, August.

Ibarra LF, Medina RA, Krawinkler H. 2005. *Hysteretic models that incorporate strength and stiffness deterioration*. *Earthquake Engineering and Structural Dynamics* 34(12), 1489-1511.

Kimura Y, Yamanishi T, Kasai K (2013). Cyclic hysteresis behavior and plastic deformation capacity for H-shaped beams on local buckling under compressive and tensile forces, *Journal of Structural and Construction Engineering*, AIJ, 78(689), 1307-1316 (in Japanese).

Krawinkler H (1996). Cyclic loading histories for seismic experimentation on structural components, *Earthquake Spectra*, 12(1): 1-12.

Krawinkler H (2009). Loading histories for cyclic tests in support of performance assessment of structural components, *Proceedings of the 3rd International Conference on Advances in Experimental Structural Engineering (3AESE)*, San Francisco, California.

Lignos, DG, Krawinkler, H, and Whittaker, AS. 2011. Prediction and validation of sidesway collapse of two scale models of a 4-story steel moment frame, *Earthquake Engng Struct. Dyn.* 40:807–825

Lignos, DG, and Krawinkler, H. 2012. *Sidesway Collapse of Deteriorating Structural Systems under Seismic Excitation*, Rep. No. TB172, The John A. Blume Earthquake Engineering Center, Stanford University, Stanford CA.

Maison B, Kasai K, and Speicher M. 2020. Loading protocols and backbone curves: U.S. and Japan perspectives, *Proceedings of 17th World Conference on Earthquake Engineering (17WCEE)*, Sendai, Japan.

Maison BF, and Speicher MS. 2016. Loading protocols for ASCE 41 backbone curves, *Earthquake Spectra*, Earthquake Engineering Research Institute, vol. 32, no. 4, November, 2513—2532. Available at: <https://www.nist.gov/publications/loading-protocols-asce-41-backbone-curves>

Maison BF, and Neuss CF, 1985, Dynamic analysis of a forty-four story building, *Journal of Structural Engineering*, American Society of Civil Engineers (ASCE), vol 111, issue 7, July.

McKenna F , and Fenves GL. 2016. *OpenSees command language manual*. Version 2.5.0, Pacific Earthquake Engineering Research Center, Berkeley, CA.

Mukaide, S, Oku, N, Matsuo, K, and Tada, M. 2016. Loading test in the range of large deformation for RHS columns with different manufacturing processes, *Steel Construction Engineering*, vol 23, issue 90 (in Japanese).

Newmark, N.M., 1962. A method of computation for structural dynamics, *Transactions, American Society of Civil Engineers*, Vol. 127, 1406-1432.

National Institute of Standards and Technology (NIST), 2017. *Recommended Modeling Parameters and Acceptance Criteria for Nonlinear Analysis in Support of Seismic Evaluation, Retrofit, and Design*, Report NIST GCR 17-917-45, April.

Speicher MS, Dukes Y, and Wong KF. 2020. *Collapse Risk of Steel Special Moment Frames per FEMA P695*, National Institute of Standards and Technology, NIST Technical Note 2084, <https://doi.org/10.6028/NIST.TN.2084>

Speicher MS, and Maison BF. 2020. Lab test confidential: seismic loading protocols, *STRUCTURE* magazine, publication of National Council of Structural Engineers Associations (NCSEA), March. Available at: <https://www.nist.gov/publications/lab-test-confidential-seismic-loading-protocols>

Suzuki Y and Lignos DG. 2020. Development of collapse-consistent loading protocols for experimental testing of steel columns, *Earthquake Engineering and Structural Dynamics*, 49(2), pp 114-131.

Suzuki Y and Lignos DG. 2021. Experimental evaluation of steel columns under seismic hazard-consistent collapse loading protocols, *Journal of Structural Engineering*, American Society of Civil Engineers, 147(4), April.

Uang, CM, Yu, QS, and Gilton CS. 2000. Effects of loading history on cyclic performance of steel RBS moment connections, *Proceedings of 12th World Conference on Earthquake Engineering* (12WCEE).

Appendix: Adaptive Model Validation

Efficacy of the adaptive component model was verified by comparison against eight physical tests (Table A1). For brevity, this Appendix shows comparisons for the reduced beam section (RBS) connection tests (tests T1 and T2), and comparisons to the other tests can be found in the Supplemental Materials file. In general, the adaptive model did a reasonable job of capturing the lab test results—especially considering its simplicity. The algorithm was implemented into a computer program made publicly available for others to study.

Table A1. Eight lab tests used to validate adaptive component model.

Test	Specimen Type	Loading Protocol	Axial Force	Source
T1	RBS	Standard	0	Uang et al. (2000)
T2	RBS	Near-fault	0	
T3	RHS	Standard	0	Mukaide et al. (2016)
T4	H-Shape	Standard	0	Kimura et al. (2013)
T5	H-Shape	Standard	0.3Py	
T6	W-Shape	Standard	0.3Py	Suzuki and Lignos (2021)
T7	W-Shape	Collapse-Consistent	0.3Py	
T8	W-Shape	Long Duration	0.3Py	

RBS Connection Lab Tests

Figure A1 shows the loading protocols and results for two RBS connection tests (W30x99 beams). Test LS-1 used a standard fully reversed protocol, and LS-3 used a protocol simulating earthquake response. No monotonic test data was available so a skeleton (backbone) curve was constructed (Figure A2a) from the test data using the method explained by Maison et al. (2020). The cyclic action curve shape is taken from the backbone curve (Figure A2b).

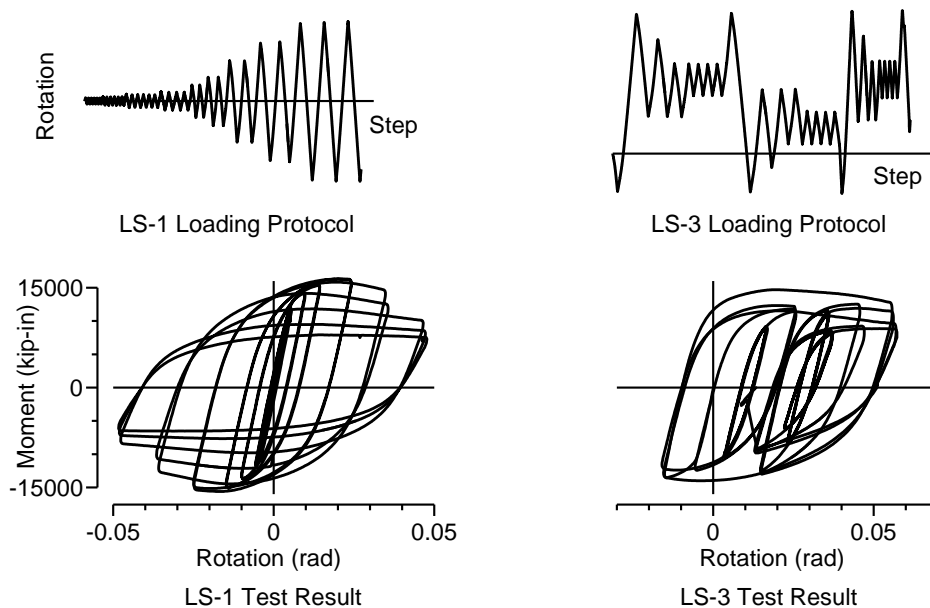


Figure A1. Test results from beam-column assemblies having reduced beam section (RBS) connections.

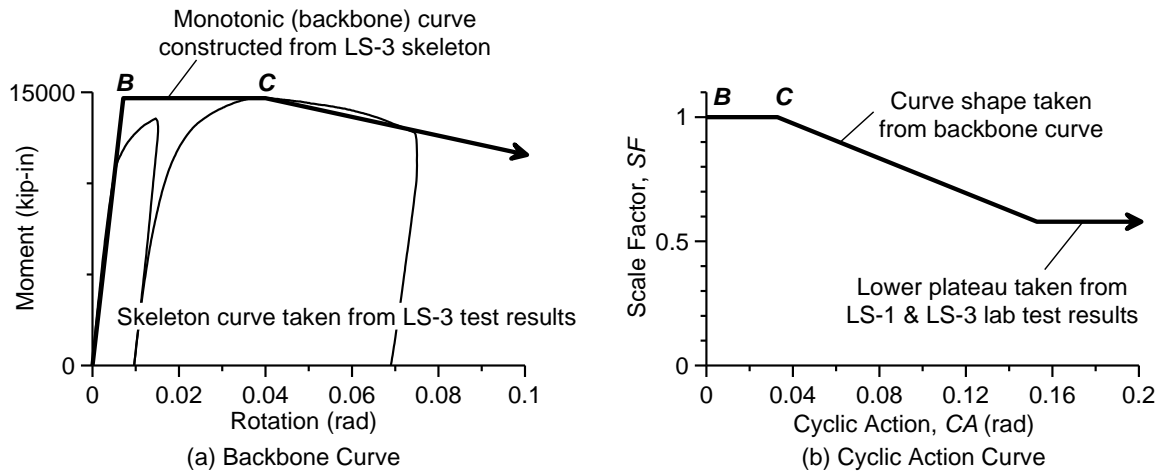


Figure A2. Adaptive model input data. (a) Backbone curve, and (b) Cyclic action curve.

The model produced hysteretic patterns generally matching the lab tests (Figures A3 and A4). Graphs using the cumulative rotation (CR) may be thought of as pseudo time histories of response as the tests proceeded. The peak moments were captured accurately in the early part of the tests, but later in the tests, the model tended to under-predict lab test moments. Likewise, cumulative work (CW) represents the energy dissipated and the model tended to under-predict in the later stages of the tests. Both trends were apparent in the other tests presented in the Supplemental Materials file. Hence, the adaptive model was conservative by under predicting strength and energy dissipation in the latter parts of the lab tests. It might be possible to tweak the backbone and cyclic action curves to achieve better lab test agreement, but this would be an iterative trial-and-error process that was considered not worthwhile. It was deemed that the adaptive model provides adequate component modeling for use in building computer models in practice.

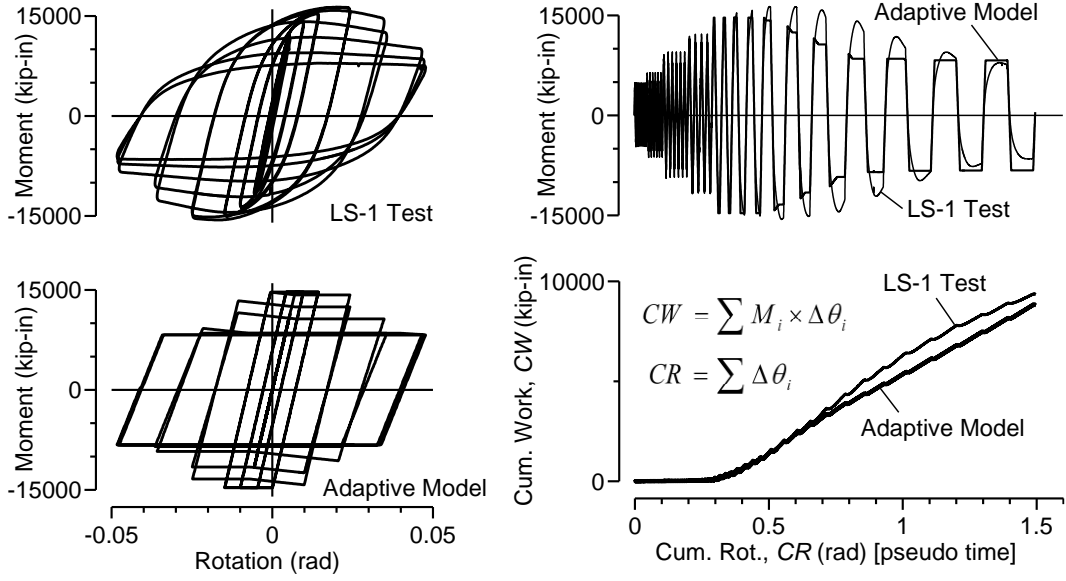


Figure A3. Comparison of adaptive model to test results for specimen LS-1.

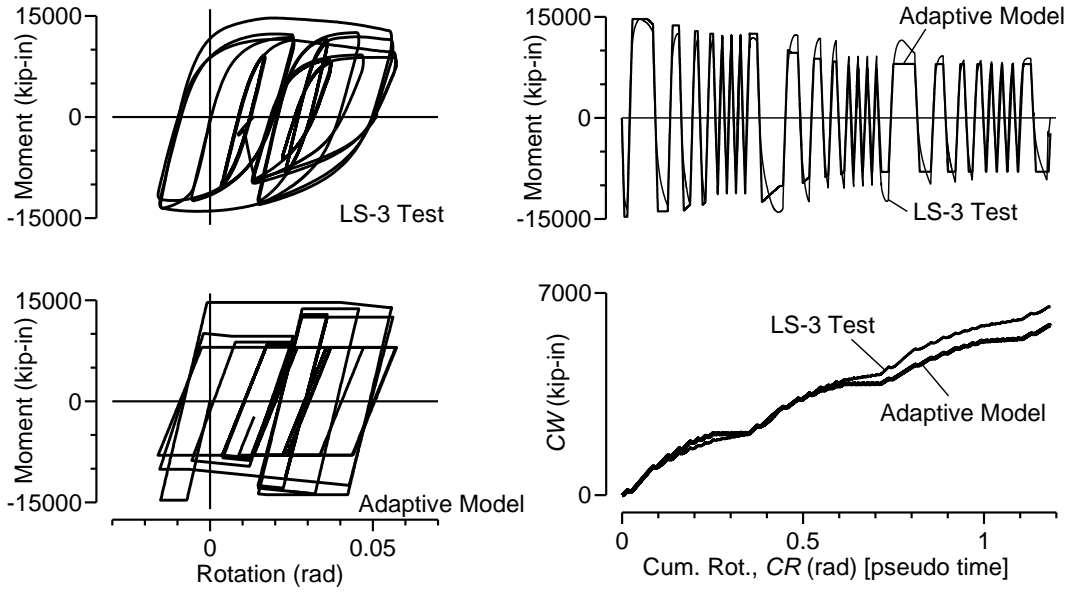


Figure A4. Comparison of adaptive model to test results for specimen LS-3.